Applied Catalysis B: Environmental 110 (2011) 25–32

Contents lists available at ScienceDirect

Applied Catalysis B: Environmental

journal homepage: www.elsevier.com/locate/apcatb

Visible light active Fe doped TiO_2 nanowires grown on graphene using supercritical CO_2

Nasrin Farhangi, Rajib Roy Chowdhury, Yaocihuatl Medina-Gonzalez, Madhumita B. Ray, Paul A. Charpentier*

Department of Chemical and Biochemical Engineering, University of Western Ontario, London, Ontario, Canada N6A 5B9

ARTICLE INFO

Article history:
Received 2 June 2011
Received in revised form 11 August 2011
Accepted 12 August 2011
Available online 2 September 2011

Keywords:
Fe doped TiO_2/graphene sheets
Super critical carbon dioxide
Sol–gel method
Band gap reduction
Electron hole recombination
Photocatalyst

ABSTRACT

Visible light driven TiO_2 photocatalyst nanowire arrays doped with Fe were grown on the surface of functionalized graphene sheets (FGSs) using a sol–gel method in the green solvent, supercritical carbon dioxide ($scCO_2$). The morphology of the synthesized catalysts was studied by SEM and TEM, which showed uniform formation of Fe doped TiO_2 nanowires on the surface of the graphene sheets, which acted as a template for nanowire growth through surface –COOH functionalities. Increasing Fe content in the nanowires gave only small changes in morphology but significantly higher BET surface areas. Optical properties of the synthesized composites were examined by UV and PL spectroscopy which showed a significant reduction in band gap with increasing Fe content, i.e. decreasing from 3.2 to 2.3 eV at 0.6% Fe. High resolution XPS and Raman analysis showed the interaction of Fe with the TiO_2 lattice and also bonding of TiO_2 with –COOH groups on the surface of the graphene sheets. The photocatalytic properties of the prepared catalysts were evaluated under visible light solar irradiation for the photodegradation of 17β-estradiol (E2), an endocrine disrupting hormone which is commonly released into aquatic environments. All prepared catalysts with different ratios of Fe were active in the visible region of the solar spectrum with the photocatalytic activity significantly enhanced with increasing Fe doping levels with a plateau at 0.6–0.8% Fe. The prepared catalysts showed higher activity than both Fe doped TiO_2 and TiO_2/FGSs composites.

1. Introduction

Heterogeneous photocatalysis has attracted considerable attention in recent years due to the potential for removing emerging environmental contaminants such as endocrine disrupting hormones (EDHs) [1–3]. TiO_2-based photocatalysts have several advantages owing to titania's abundance, non-toxicity, low-cost, unique optical-electronic properties and long term thermodynamic stability [4]. Nanostructured TiO_2 has been used for various environmental applications including degrading organic pollutants [5], dye-sensitized solar cells [6], self cleaning surfaces [7], water splitting [8] and antimicrobial coatings [9,10]. However, there are limitations for using commercial nano TiO_2 in these applications (e.g. Degussa P25) as TiO_2 nanoparticles easily agglomerate, have low surface areas, and give a low efficiency because of TiO_2's wide band gap (3.2 eV) which is only active in the UV region of the solar spectrum [11]. Current research efforts are focussed on enhancing photocatalytic degradation using visible light ($400\,nm < \lambda < 760\,nm$) which is often unused in UV-photocatalysis, although a target for next-generation photocatalytic processes.

For extending the absorbance of TiO_2 into the visible region, doping with transition metals is a useful technique [12]. For doping of TiO_2, various metal ions have been used, but among them, Fe^{3+} is considered as a strong candidate as it has a similar radius to Ti^{4+} and can easily fit into the crystal lattice of TiO_2 [12–14]. Moreover, the redox potential (energy differential) of Fe^{2+}/Fe^{3+} is close to that of Ti^{3+}/Ti^{4+}, resulting in shifting its optical absorption into the visible region [12,14]. Another common method for increasing the photocatalytic efficiency of TiO_2 is immobilization of TiO_2 powder on a co-adsorbent surface such as zeolites [15], alumina [16], silica [17] or activated carbon [18]. Among these, carbonaceous materials are of tremendous current interest due to their unique pore structure, electronic properties, adsorption capacity and acidity. These materials include activated carbon [19], carbon nanotubes, and more recently graphene [20–23]. Graphene can be synthesized inexpensively from earth abundant graphite [24] providing larger specific surface areas similar to activated carbon and carbon nanotubes. This facilitates pollutant adsorption enhancing the photocatalytic efficiency by TiO_2. In addition, functional groups such as alcohol and carboxylic acids can be introduced onto the graphene surface [25]. Groups such as –COOH allow for both

* Corresponding author. Tel.: +1 519 661 3466; fax: +1 519 661 3498.
E-mail address: pcharpentier@eng.uwo.ca (P.A. Charpentier).

0926-3373/$ – see front matter © 2011 Elsevier B.V. All rights reserved.
doi:10.1016/j.apcatb.2011.08.012

adsorption of specific pollutants and potentially can be exploited as a selective template for sol–gel nanowire growth on the graphene surface. Hence, graphene can potentially harness and stabilize different semiconductors on its surface to produce more stable and porous photocatalysts [26,27].

There are a few reports for the preparation of graphene-TiO_2 composites and also their corresponding applications. P25-graphene composites synthesized by a hydrothermal method were used as a photocatalyst for photodegradation of methylene blue. A remarkable enhancement in reaction rate was observed compared to P25 and P25-CNTs [22]. Titanium oxide nanoparticle-graphene oxide (TiO_2-GO) and titanium oxide nanoparticle-reduced graphene oxide (TiO_2-RGO) composites were synthesized by Lambert et al. via the hydrolysis of TiF_4 at 60 °C [28].

In this work, we show that Fe doped TiO_2 can be grown on the surface of functionalized graphene sheets (FGSs) containing –COOH functional groups using supercritical carbon dioxide ($scCO_2$) as the enabling solvent. TiO_2 nanowires were prepared previously in $scCO_2$ using Ti alkoxides and acetic acid as the polycondensation agent with the mechanism of wire formation examined [29]. $ScCO_2$ is an inexpensive, green alternative to conventional organic solvents [29,30] which is inexpensive, environmentally benign and non-flammable with low viscosity, zero surface tension and high diffusivity which are favourable for synthesizing fine and uniform nanomaterials. $ScCO_2$ can facilitate doping in titania [31,32] and has been used to enhance exfoliation of graphene sheets [33]. No drying process is required as complete removal of excess acetic reaction ingredients is easy by supercritical fluid extraction, maintaining the porous nanostructure [29,30]. The resulting materials from this study are examined with visible light for the photocatalytic degradation of 17β-estradiol (E2).

2. Experimental

2.1. Materials

Graphite flake nominally sized at 7–10 μm was provided from Alfa Aesar. Fuming nitric acid (>90%), sulphuric acid (95–98%), potassium chlorate (98%), titanium isopropoxide (99.999%) trace metals basis, iron chloride, $FeCl_3$, titanium (IV) oxide nanopowder (99.7%) trace metals basis (anatase), E2 ($C_{18}H_{24}O_2$, CAS registry number: 50-28-2) and hydrochloric acid (37%) were purchased from Sigma–Aldrich and used as received.

2.2. Methods

2.2.1. Preparation of functionalized graphene sheets (FGSs)

Graphite oxide was prepared using the Staudenmaier method [34] with graphite (5 g) reacted with concentrated nitric acid (45 mL) and sulphuric acid (90 mL) with potassium chlorate (55 g). Potassium chlorate was added slowly over 15 min to avoid sudden increases in temperature. The mixture was stirred at room temperature for more than 3 days. After reaction completion, the viscous dark green mixture was added to excess water, washed with a 5% solution of HCl, and then repeatedly washed with water until the pH of the filtrate was neutral. The prepared graphite oxide was kept in a vacuum oven at 80 °C until use. Then, the graphite oxide powder was placed in a quartz tube with an inlet and outlet for continuously passing nitrogen gas. The tube was then inserted into a tubular furnace preheated to 1050 °C and kept at this temperature for 30 s, and then removed. The graphite oxide was reduced and expanded to form FGSs.

2.2.2. Preparation of Fe doped TiO_2/graphene sheets composites

TiO_2 nanowires were successfully synthesized on the surface of graphene sheets in supercritical carbon dioxide ($scCO_2$) using acetic acid/titanium isopropoxide (AcOH/TIP: 4), 60 °C and 5000 psi as previously determined as the optimized experimental conditions [35]. In a typical experiment, first FGSs (0.05 g) were placed in a 10 mL high pressure view cell followed by quick addition of titanium isopropoxide (1 mL), $FeCl_3$ dissolved in isopropanol (Fe percentage is the weight ratio of $FeCl_3$:TIP), acetic acid (4 mL) and CO_2 to the desired pressure and temperature. A magnetic stirrer with TFE stir bar was used for mixing the reaction mixture. It was found that the mixture of iron chloride/isopropanol, functionalized graphene sheets, titanium isopropoxide and acetic acid were miscible with CO_2 at 60 °C and 5000 psig pressure. The stirrer was stopped after 24 h while normally several days of aging were required for complete reaction. After aging, the formed gel was washed continuously using 80 mL of CO_2 at a rate of approximately 0.5 mL/min, followed by controlled venting at 0.5 mL/min to prevent collapse of the solid network. The resulting powder was then calcined at 450 °C in air (tubular furnace) using a heating rate of 10 °C/min for 2 h. The calcined powder was kept in a vacuum oven at 80 °C.

2.3. Characterization

The nanostructured morphologies of the samples were examined using scanning electron microscopy (SEM) micrographs (Model LEO 1530) and transmission electron microscopy (TEM) (Model JEOL 2010F) with a 200 keV Schottky field emission microscope (TEM/STEM). Samples for SEM imaging were prepared by applying the powder directly to a carbon adhesive tape. For TEM analysis, the powdered samples were dispersed in methanol by sonication and then placed on a copper grid covered with holey carbon film and dried by normal evaporation. Structural analysis of the samples was performed using an X-ray powder diffractometer (Rigaku Miniflex XRD, Texas, USA), fitted with a rotating sample holder, a scintillation counter detector and a divergent beam utilizing a Cu Kα source of X-rays (λ = 1.5418 Å). Raman analysis was performed using a Kaiser optical systems (RXN1-785) with 5 times exposure and 20 times accumulation. The XPS analyses were carried out with a Kratos Axis Ultra spectrometer using a monochromatic Al Kα source (15 mA, 14 kV). Photoluminescence (PL) spectra were carried out using a PTI Quantamaster 50 spectrophotometer with the Xenon lamp (75 V). UV–Vis spectra were performed with a Shimadzu 3600 deuterium arc lamp and two different detectors (PMT and PbS). An integrating sphere was utilized in order to measure the diffuse reflectance of the material.

2.4. Photocatalytic activity measurements

Photodegradation of 17β-estradiol (E2) as a model endocrine disrupting compound (EDC) was investigated under visible solar irradiation ($\lambda \geq 420$ nm). A solar simulator (Model: SS1KW, Sciencetech) with a 1000 watt xenon arc lamp equipped with an air mass filter (AM 1.5G) with a special UV cut-off filter ($290 < \lambda < 420$ nm) provided the visible light source. Typically, a mixture of aqueous E2 solution (5 μg/L) and 0.5 g/L of catalyst was vigorously stirred for 30 min to establish an adsorption/desorption equilibrium in the dark. Then the reaction solution was irradiated under visible light in an open water-jacketed vertical photo-reactor which was placed on a magnetic stirrer during all experiments, under aerated conditions [1]. The temperature of the reactions was controlled at 22 ± 1 °C using a controlled temperature bath. At given time intervals, 5 mL aliquots were sampled and centrifuged to remove the particles. The filtrates were analyzed by HPLC (ICS 300, Dionex), using a PDA UV detector, connected to Chromeleon software. Separations were carried out with an Acclaim 120 C18 reversed-phase column (150 mm × 4.6 mm i.d., 5 μm particle size, Dionex, USA). The injection volume was 40 μL from a 2 mL HPLC

Table 1
Synthesis conditions, morphology, BET surface area, pore volume, and pore size distribution of TiO_2, Fe doped TiO_2/FGSs composites (0.1%, 0.2%, 0.4%, 0.6% and 0.8%).

Materials	BET surface area (m^2/g)	Total pore volume (cm^3/g)	Average pore size (nm)	Band gap (eV)	Morphology
TiO_2 anatase (commercial)	50	–	–	3.2	Nanoparticles
TiO_2/FGSs	118	0.12	45.3	2.9	Nanowires
Fe/TiO_2 (0.4%)	156	0.11	38.7	2.5	Nanoflower
Fe/TiO_2/FGSs (0.1%)	128	0.10	41.6	2.82	Nanowires on the sheet
Fe/TiO_2/FGSs (0.2%)	174	0.13	39.3	2.53	Nanowires on the sheet
Fe/TiO_2/FGSs (0.4%)	214	0.20	37.48	2.42	Nanowires on the sheet
Fe/TiO_2/FGSs (0.6%)	256	0.23	31.5	2.25	Nanowires on the sheet
Fe/TiO_2/FGSs (0.8%)	297	0.29	29.2	2.25	Nanowires on the sheet

All materials prepared in $scCO_2$ (60 °C, 5000 psi), FGSs/TIP: 1:20, AcOH/TIP: 4 and calcined at 450 °C.

vial, capped and sealed with PTFE lid. The mobile phase was a mixture of AcN and Milli-Q water (50:50, v/v) at a flow rate of 1 mL/min. The column temperature was maintained at 30 °C and detection wavelength was set at 280 nm, the maximum absorbance of E2. The retention time of E2 in the HPLC column was 5.33 min. In the kinetic degradation experiments of E2, the initial concentration was 5 ± 0.3082 μg/L. The maximum degradation was kept to 90%, i.e. the final concentration of E2 measured was approximately 0.5 μg/L, which was within the limits of the determined calibration curve (see Supporting Document).

3. Results and discussion

3.1. Characterization of synthesized materials

Different percentages of Fe doped TiO_2/functionalized graphene sheets (FGSs) and Fe doped TiO_2 were synthesized in $scCO_2$. The experimental conditions and resulting properties of the synthesized materials are summarized in Table 1.

The morphology and particle size of the Fe doped TiO_2/FGSs materials synthesized via the examined acid-modified sol–gel technique in $scCO_2$ were assessed by SEM and TEM analysis.

In Fig. 1, a typical SEM image of Fe doped TiO_2/FGSs (0.2% Fe – Fig. 1a) and (0.6%Fe – Fig. 1b) is shown. Increasing the amount of Fe was not found to change the morphology of nanowires on the surface of the graphene sheets significantly; however, the nanowires with higher Fe contents appear more porous. As shown in Table 1, the BET determined surface areas of the Fe doped TiO_2/FGSs samples were found to be significantly higher than the undoped TiO_2 nanowires on the graphene sheets, and directly increased with increasing Fe content. Introducing Fe to the titania sol–gel mixture for growth on the graphene sheets increases the surface area by producing more pores inside the composites with smaller pore sizes enhancing the mesoporous structure. Lucky and Charpentier synthesized Fe doped TiO_2 nanofibers in $scCO_2$ without graphene, reporting similar results [31].

In Fig. 1c and d, TEM images show that the diameter of the TiO_2 nanowires is less than 20 nm. Good dispersion of TiO_2 nanowires on the graphene sheets can be observed along with

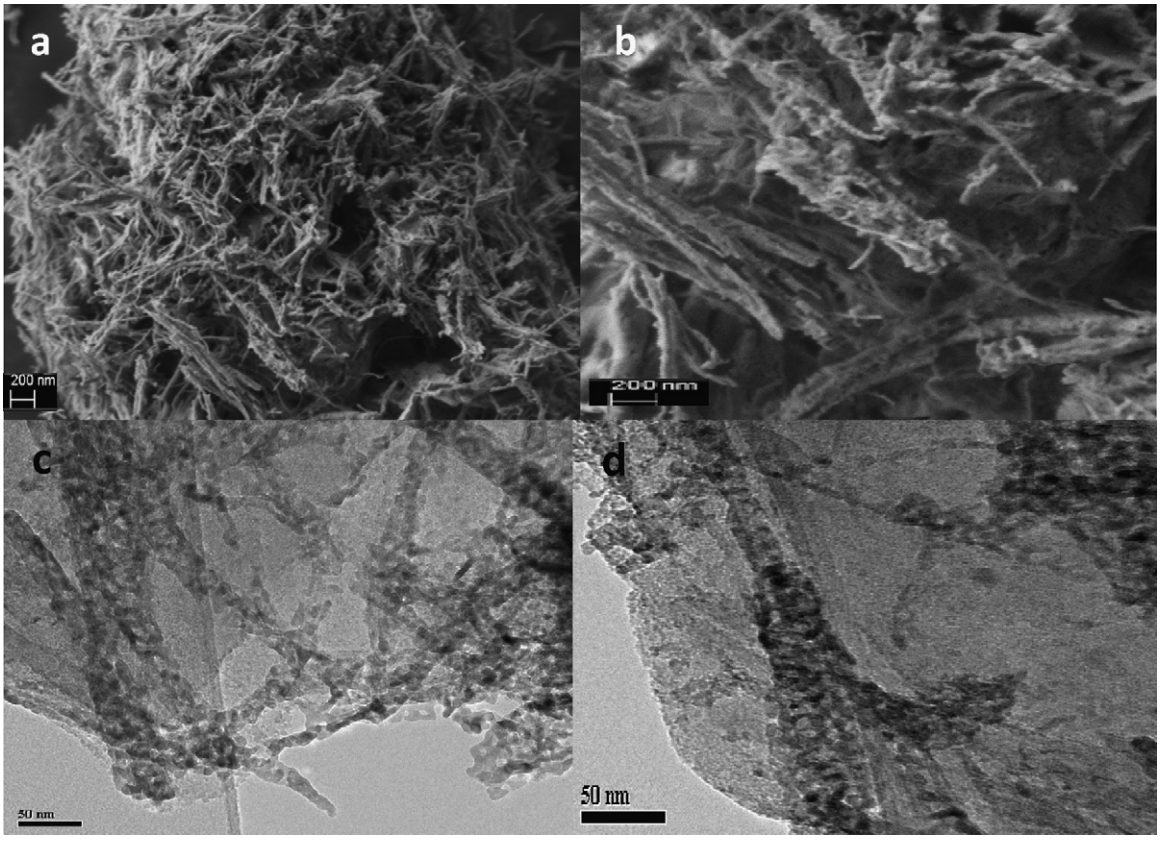

Fig. 1. SEM images of (a) Fe doped TiO_2/FGSs 0.2% (200 nm scale), (b) 0.6% (200 nm scale); TEM images of Fe doped TiO_2/FGSs (c) 0.2% (50 nm) and (d) 0.6% (50 nm).

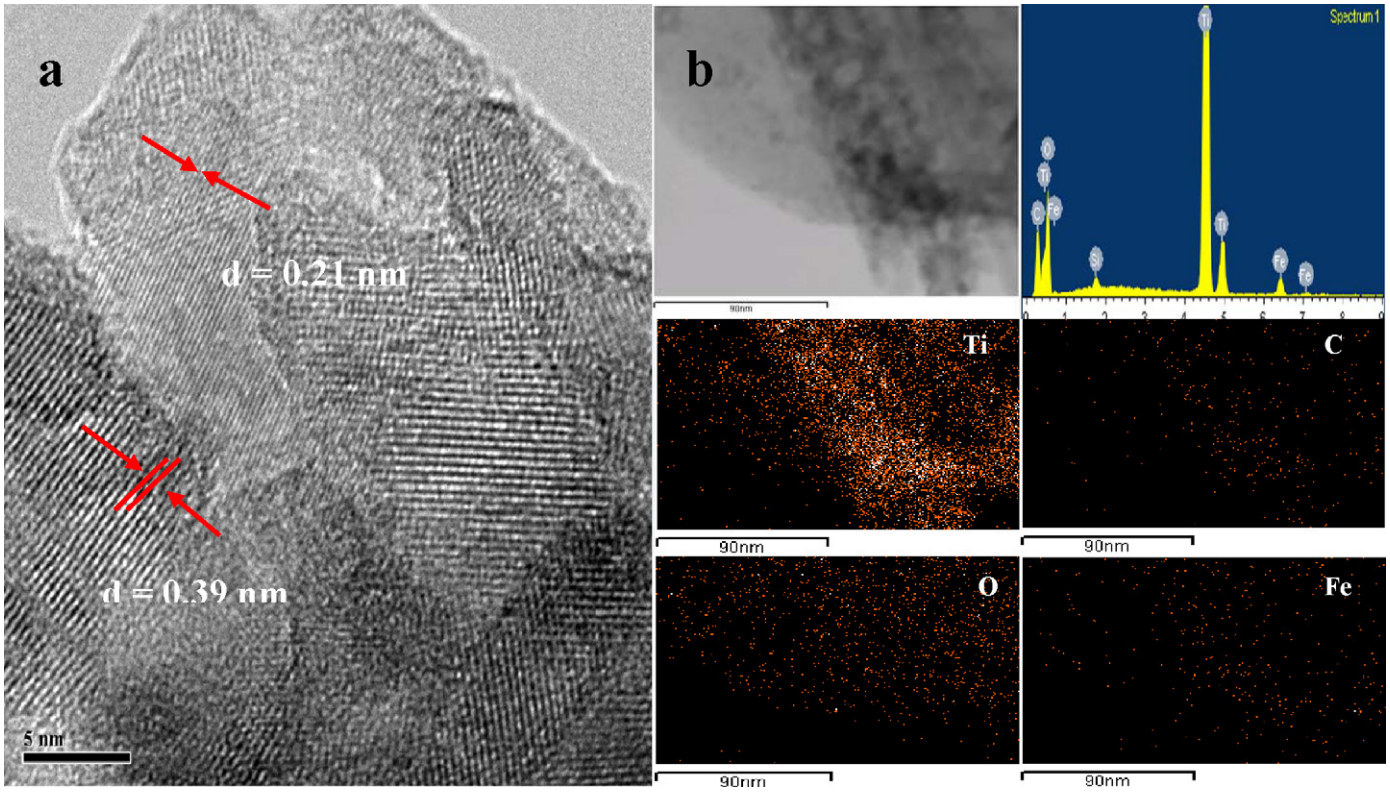

Fig. 2. (a) HRTEM image of Fe doped TiO_2/FGSs (0.2%), (b) HRTEM-EDS elemental mapping of Fe doped TiO_2/FGSs assembly.

excellent contact between the graphene sheet and wires. SEM images of 0.2% Fe doped TiO_2 and TiO_2/FGSs are available in the supporting information for comparison. When graphene sheets were not used as the support, the morphology of synthesized materials showed a flower-like structure. TiO_2/FGSs composites also showed similar structure as Fe doped TiO_2/FGSs with less porosity.

The HRTEM micrographs of the lattice image of 0.2% Fe doped titania/graphene calcined at 450 °C is given in Fig. 2a, showing uniform dispersion of anatase with *d*-spacing 0.39 nm (1 0 1) as well as some rutile with *d*-spacing 0.21 nm (1 1 1) [36]. There was no Fe detected in the HRTEM micrographs indicating that all the Fe is contained within the TiO_2 lattice. However, the *d*-spacing increased which is in good agreement with the XRD data as explained later confirming expansion of the TiO_2 lattice. In Fig. 2b, the EDX spectra with elemental analysis of this sample shows 25.6% of C, 59.1% of O, 14.1% of Ti and 1.2% of Fe on the surface. Elemental mapping was measured in several selected sample areas confirming uniform dispersion of Ti, C, O and Fe in the synthesized material.

The optical absorption spectra obtained by the diffuse reflection method for TiO_2 nanowires and different percentages of Fe doped TiO_2 on the surface of graphene sheets prepared in $scCO_2$ are shown in Fig. 3a. By adding Fe to the TiO_2/FGSs composites, a noticeable shift in the absorption edge into the visible light region was observed (to 550 nm). As shown in the figure, the band gap energy of doped TiO_2 was obtained by drawing a tangent line on the edge of the UV spectra to determine the cut off wavelength at $y = 0$ [37,38]. Pure TiO_2 anatase has a band gap of 3.2 eV with the band gap decreasing with an increasing amount of Fe in the composites, with the smallest band gap measured of 2.25 eV for 0.6% Fe doping. Further increasing of the Fe concentration to 0.8% did not further decrease the band gap. In Fig. 3b, the diffuse reflectance UV–Vis spectra of TiO_2 nanowires (1), 0.4% Fe doped TiO_2 (2) and 0.4% Fe doped TiO_2/FGSs (3) prepared in $scCO_2$ are compared. By adding graphene to the system, the band gap of Fe doped TiO_2 decreased from 2.5 to 2.4 eV attributed to enhanced electron hole recombination of TiO_2 and graphene. In Fig. 3c, the UV spectra of TiO_2 with band gap of 3.2 eV are compared to TiO_2/FGSs with a band gap of 2.9 eV.

The photoluminescence (PL) spectra of TiO_2 and the $scCO_2$ synthesized composites are shown in Fig. 4. TiO_2 (anatase) has a characteristic broad peak at around 540 nm as shown in spectra a [39]. Although the PL intensity decreased in both the Fe doped TiO_2 nanowires and the TiO_2 nanowires/FGSs composites compared to anatase alone, the reduction is significantly greater in the Fe doped TiO_2/FGSs composites. When Fe doped TiO_2 nanowires are in contact with the graphene sheets, excited electrons have a lower chance for recombination resulting in a decreased band gap and enhanced visible light activity. These results help to confirm the UV–Vis results.

The structure of Fe doped TiO_2/FGS composites that was synthesized using the sol–gel method in $scCO_2$ appear to be amorphous; however, by thermal annealing at 450 °C, depending on dopant loading, anatase or a mixture of anatase and rutile TiO_2 was obtained. In Fig. 5, XRD spectra of different percentages of Fe doped TiO_2/FGSs are shown. No obvious peaks for Fe could be detected indicating that the Fe ions were fully integrated into the TiO_2 crystal lattice as earlier observed by the HRTEM results. In the 0.2% Fe doped TiO_2/FGSs (Fig. 5a), a mixture of anatase and rutile TiO_2 is observed. By increasing the concentration of Fe to 0.4% (Fig. 5b), the amount of rutile phase decreased. By increasing the concentration of Fe further to 0.6% and 0.8% (Fig. 5c and d), only anatase phase was obtained. These results indicate that the specific concentration of Fe ions can affect the rate of anatase-rutile phase transformation. By increasing the amount of dopant in TiO_2, the oxygen vacancies

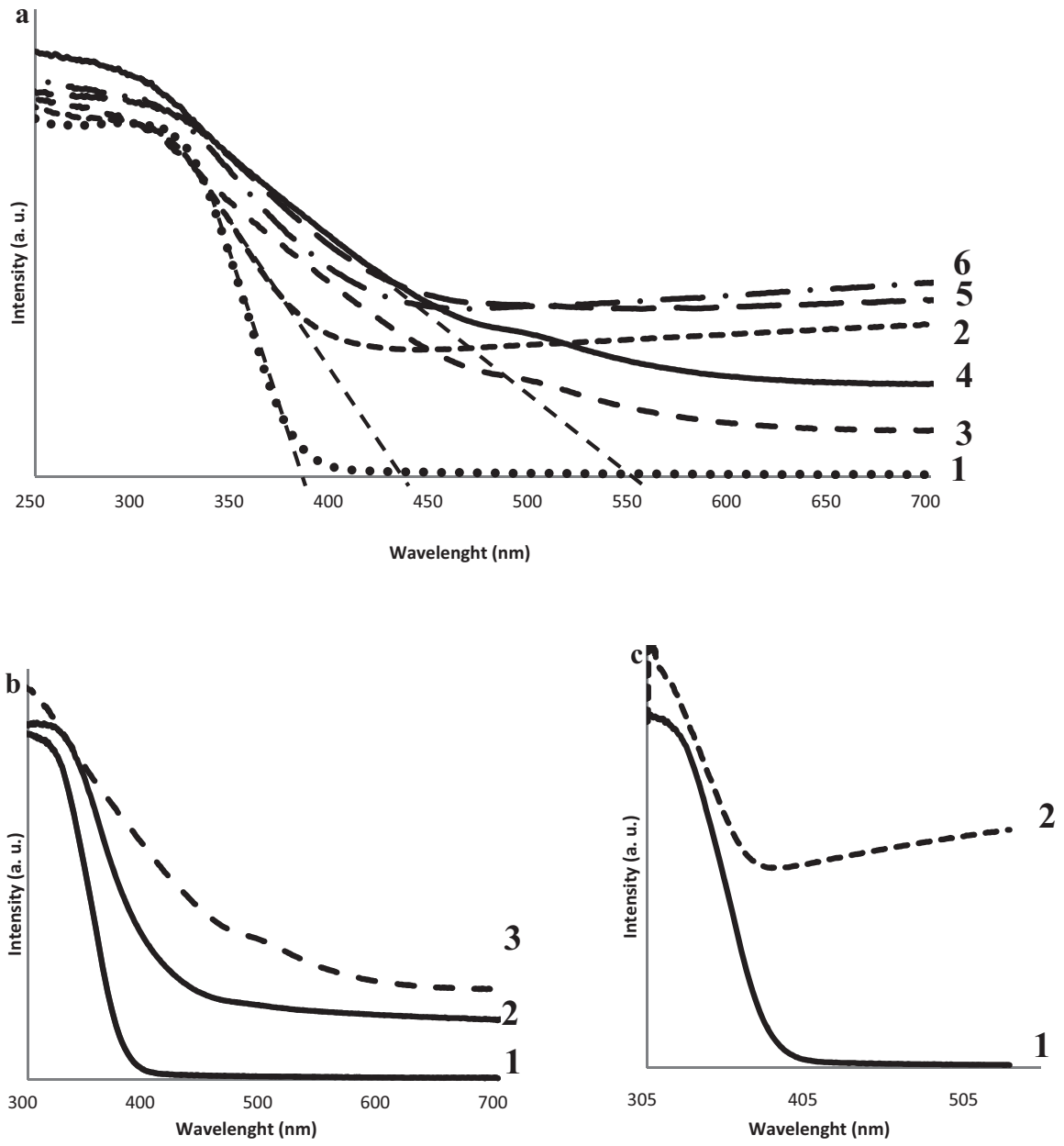

Fig. 3. Diffuse reflectance UV–Vis spectra of: (a) (1) TiO_2 anatase; Fe doped TiO_2/FGSs (2) 0.1%, (3) 0.2%, (4) 0.4%, (5) 0.6% (5) and (6) 0.8%; (b) (1) TiO_2, (2) 0.4% Fe doped TiO_2 and (3) 0.4% Fe doped TiO_2/FGSs; (c) (1) TiO_2 and (2) TiO_2/FGSs prepared in $scCO_2$.

increased and more anatase phase can result from A-R phase transformations involving a contraction of the oxygen structure [40]. Choi et al. studied the effect of different dopants on A-R phase transformation and suggested that the addition of dopants with small radii could be directly integrated into the TiO_2 crystal lattice and by introducing more oxygen sites in the lattice, more anatase TiO_2 was formed [41]. On the other hand, an increase in the Fe content leads to a shift of the (1 0 1) and (2 0 0) reflections to lower angles corresponding to the unit cell expansion due to the replacement of Ti^{4+} ions by slightly larger Fe^{3+} ions. The same changes in *d*-spacing with increasing Fe content were also observed in the HRTEM images of the doped materials.

Graphite has two well known characteristic bands in the Raman spectra; the strong G band at 1575 cm^{-1} and the weak D band at approximately 1355 cm^{-1} [42]. After oxidation of graphite to graphite oxide and then thermal expansion to FGSs, both the G and D bands change noticeably. A higher disorder in graphite resulted in a broader G band, as well as a higher intensity, broader D band compared to that of the G band (Supporting Information) [42]. After functionalization of FGSs with TiO_2, the D/G ratio, which represents the degree of functionalization, increased dramatically indicating good attachment of the TiO_2 nanowires to the surface of the graphene sheets (D/G ratio ~ 2.5) as shown in Fig. 6. The main characteristic peak of anatase TiO_2 appears at 145 cm^{-1} which is attributed to the main E_g anatase vibration mode [42]. Moreover, the presence of crystalline TiO_2 in the composite s is confirmed by the vibration peaks at 400 cm^{-1} (B_{1g}), 519 cm^{-1} (A_{1g}) and 640 cm^{-1} (E_g) [43]. After Fe doping, the Raman spectra did not change significantly (D/G ratio ~ 2.6) attributed to all the Fe being integrated into the TiO_2 lattice. The only change is a shift of the TiO_2 peak to the higher wavenumbers in the Fe doped composites, indicating an increase in the surface oxygen vaccancies [44].

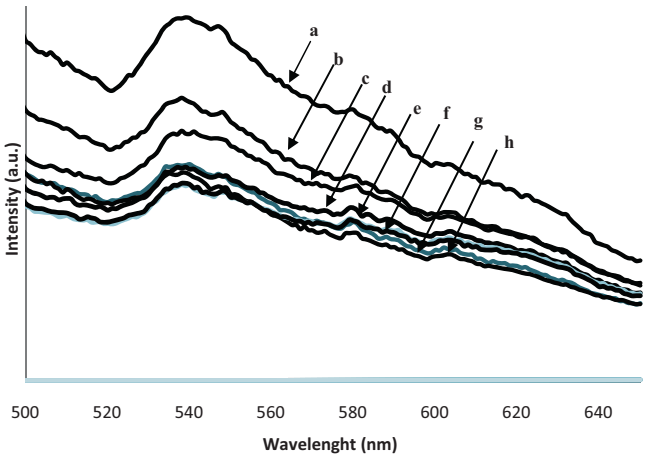

Fig. 4. Photoluminesence spectra of (a) TiO_2 (anatase), (b) TiO_2/FGSs composites, (c) Fe doped TiO_2, (d) 0.1%, (e) 0.2%, (f) 0.4%, (g) 0.6% and (h) 0.8% Fe doped TiO_2/FGSs composites.

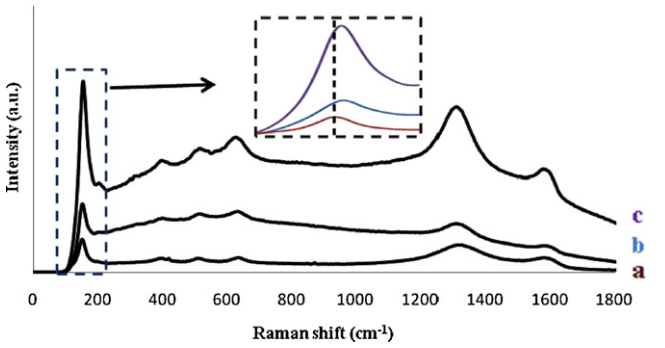

Fig. 6. Raman spectra of (a) TiO_2/FGSs composites, (b) Fe doped TiO_2/FGSs (0.2%) and (c) (0.6%).

Zhu et al. prepared Fe-doped nanocrystalline via a nonhydrolytic sol–gel method and observed a similar shift in the Raman study [45].

In the XPS spectra of FGSs, 90% carbon and 10% oxygen were detected. In high resolution XPS of C1s (see Supporting Document), four different peaks were observed at 284.7, 286.2, 287.7 and 289.3 eV which correspond to the (C–C, C=C), (C–H), (C–OH, C–O–C) and C=O functionalities, respectively. Akhavan studied the XPS spectra of graphite oxide and thermal expanded graphene sheets at different temperatures and reported similar results [46]. The XPS spectra of 0.6% Fe doped TiO_2/FGSs shows 6.1% Fe 2p, 54.7% O1s, 18.7% Ti 2p and 20.5% C1s. In high resolution of C1s, four different peaks of FGSs are still available but the intensity of peaks which represented C=O and C–OH decreased. The peak at 289.25 eV corresponds to C=O also shifted to lower energy (288.80 eV) implying coordination bonding between Ti and carboxylic acids on the surface of the graphene sheets. The O 1s main peak at 530.3 eV is assigned to the metallic oxides (Ti–O), which is consistent with the binding energy of O^{2-} in the TiO_2 lattices. The peak at 533.40 eV corresponding to O–H disappeared, but the peak at 531.38 eV corresponding to the carbonyl group is still observable [46]. The Ti 2p3/2 and Ti 2p1/2 for Fe doped TiO_2 on the graphene surface are located at binding energies of 458.36 eV and 464.1 eV, respectively, which is consistent with the values of Ti^{4+} in the TiO_2 lattices [14]. The peaks at 711.9 eV and 724.6 eV are assigned to 2p3/2 and 2p1/2 of Fe^{3+}, respectively. These data exhibit a slightly positive shift compared to those in Fe_2O_3 (710.7 eV for 2p3/2 and 724.3 eV for 2p1/2). The positive shift of the Fe2p level binding energy may be due to transferring the electrons from Fe^{3+} into the TiO_2 lattice and the formation of Fe–O–Ti bonds in the composite [14].

3.2. Visible-light photocatalytic activity

The photocatalytic activities of the different iron doped (0%, 0.2%, 0.4%, 0.6% and 0.8%) TiO_2 nanowire/graphene sheets and also Fe doped TiO_2 samples were evaluated through the photodegradation effects of E2 (Fig. 7) in aqueous solution using a solar simulator with a filter to block UV light allowing only visible irradiation ($\lambda > 420$ nm). We found no photodegradation of E2 in the presence of pure nano TiO_2 under visible irradiation as expected, as TiO_2 only produces $OH^{\bullet}$ in the presence of UV radiation. The results for the different Fe doped TiO_2 nanowires/graphene sheets and also Fe doped TiO_2 samples are shown in Fig. 7. The degradation rate in visible light increased directly with increasing Fe dopant level, although only a marginal

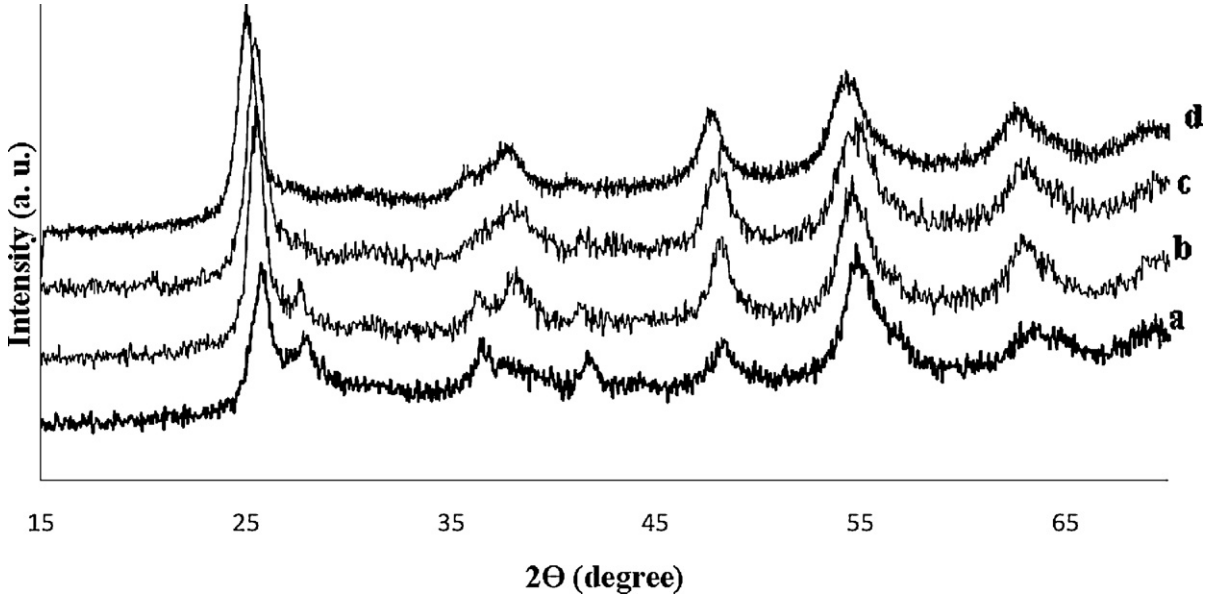

Fig. 5. XRD pattern of (a) 0.2%, (b) 0.4%, (c) 0.6% (c) and (d) 0.8% of Fe doped TiO_2/FGSs composites prepared at 60 °C and 5000 psi and calcined at 450 °C.

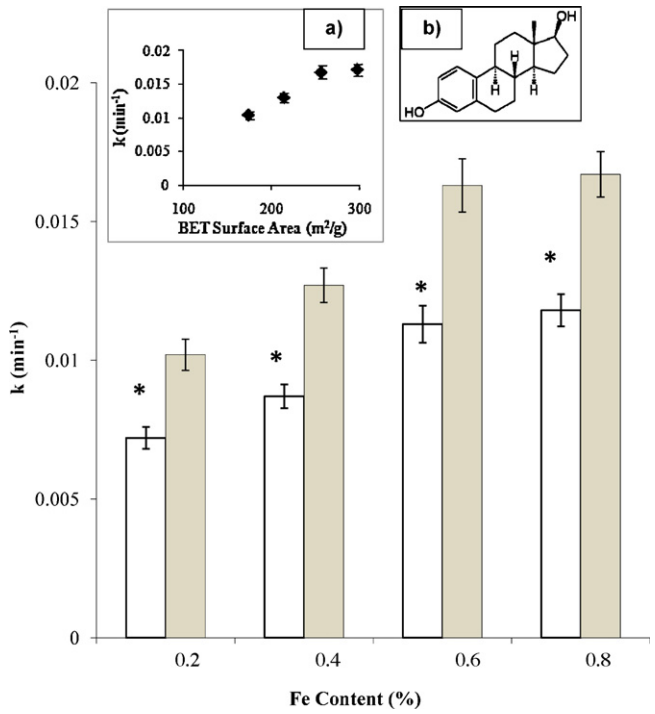

Fig. 7. Photocatalytic degradation rate constant of E2 using Fe doped TiO_2 samples on graphene sheets (*Fe/TiO_2 samples without graphene). Inset: (a) the effect BET surface area of Fe doped TiO_2 graphene sheets on the photocatalytic degradation rate constant of E2, and (b) structure of 17β-estradiol (E2).

increase in rate occurred from 0.6% to 0.8%, indicating the presence of an optimal loading. As shown in Fig. 7, the Fe doped TiO_2 nanowire/graphene assemblies show higher photocatalytic activity than the Fe doped TiO_2 composites without graphene, attributed to both enhancing the pollutants adsorption to the graphene surface along with graphene helping to lower titania's band gap energy.

The degradation kinetics are further studied at 0.6% Fe loading, as shown in Fig. 8. There was no photodegradation of E2 in the presence of visible light (λ > 420 nm) due to direct photolysis (i.e. no catalyst), because E2 does not have any absorbance in the visible wavelength region [1]. The experiments in the presence of photocatalyst illustrate that 30 min was sufficient to reach the adsorption equilibrium. The degradation of E2 could occur because of photocatalytic reactions in the presence of catalyst under visible light (λ > 420 nm), with E2 almost completely degraded in less than 150 min.

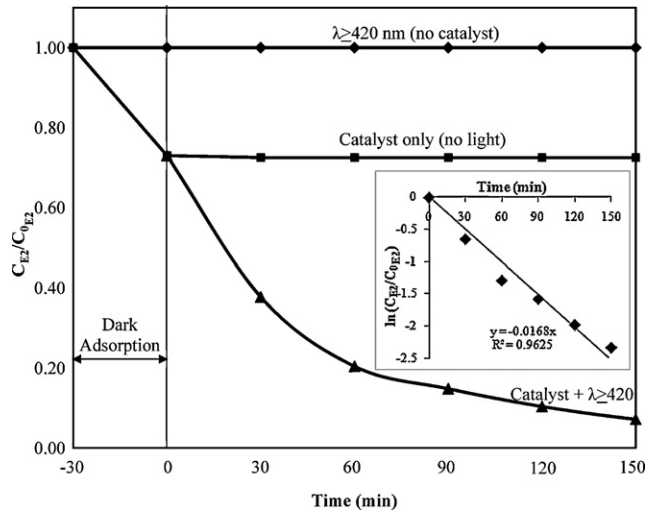

Fig. 8. Photocatalytic degradation and kinetic study of E2 under visible solar irradiation (λ > 420 nm). $C_{0_{E2}} = 5$ μg/L, pH = 6.5, solar intensity = 1 SUN, catalyst: 0.6% Fe doped TiO_2 nanowires/graphene sheets and irradiation time = 150 min.

Reaction kinetics for adsorbing species are often described in terms of the Langmuir–Hinshelwood model, which can be expressed as:

$$-\frac{dC}{dt} = k_r \frac{k_a C}{1 + k_a C} \quad (1)$$

where $(-dC/dt)$ is the degradation rate of E2, C is the concentration of E2 in the solution, t is reaction time, k_r is the reaction rate constant, and k_a is the adsorption coefficient of the reactant. $k_a C$ is negligible when the value of C is very small. As a result, Eq. (2) can be described as pseudo-first order kinetics. Setting Eq. (2) at the initial conditions of the photocatalytic experiment, when $t = 0$, $C = C_0$, it can be described as:

$$\ln\left(\frac{C_0}{C}\right) = k_{app} \times t \quad (2)$$

As shown in Fig. 8-inset, the photocatalytic degradation followed pseudo-first-order reaction kinetics in the studied concentration range. The half-life of E2 can then be calculated as per Eq. (3):

$$t_{1/2} = \frac{\ln 2}{k_{app}} \quad (3)$$

The calculated half-life of E2 at 1 sun intensity for 0.6% Fe doped TiO_2 nano wires/graphene sheet was only 41 min, whereas it was about 10 h in the absence of catalyst due to direct photolysis under 1 sun solar irradiation (AM 1.5G) using similar experimental conditions [1,2].

The enhancement in photocatalytic performance of the Fe-doped TiO_2/graphene samples can be explained by the higher surface area with mesoporous structure, lowered band gap and defects induced by Fe doping [47,48]. Although the measured band gap energy of both the 0.6% and 0.8% Fe doped TiO_2 nanowire/graphene assemblies was 2.25 eV, the surface area of the 0.8% Fe was 297 m^2/g compared to 256 m^2/g for the 0.6% Fe catalyst. The higher surface areas with mesoporous structure favours the adsorption of reactant molecules, as well as light absorbance. Fig. 7 inset plots k versus the BET surface area of the nanoassembles showing a plateau in the rate with surface area. In addition, the increase of defects which were observed by the HRTEM images could capture more photoelectrons and thus reduce their recombination with photo induced holes. These factors would enhance the quantum efficiency, leading to the observed higher photocatalytic activity.

A proposed mechanism for charge transfer in the Fe doped TiO_2/FGSs composites is shown in Scheme 1 in which the Fe doped TiO_2 nanoparticles are in intimate contact with FGSs. The FGSs have a work function around 4.2–4.5 eV [49], in which excited electrons from the Fe doped TiO_2 anatase conduction band can transfer to its (FGSs) conduction band, resulting in narrowing the band gap, reduction in photoluminescence intensity, charge separation, stabilization, and hindering charge recombination. Moreover, Fe doped TiO_2/graphene photocatalysts can absorb more visible light which is favoured for photocatalytic reactions. In addition, when Fe doped TiO_2 were grown on the surface of graphene sheets, higher surface area photocatalysts were obtained; pollutant (E2) molecules were trapped on graphene pores, then Fe doped TiO_2 degrade them more efficiently in the visible area.

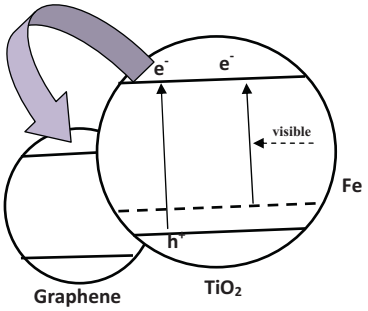

Scheme 1. Schematic of a proposed model for Fe doped TiO_2/FGSs with enhanced visible light photocatalytic reactivity.

4. Conclusions

Fe doped TiO_2 nanomaterials on the surface of graphene sheets were successfully synthesized by a simple sol–gel process using the green solvent, $scCO_2$. Fe doped TiO_2 nanowires were uniformly formed on the surface of graphene sheets with increasing surface area confirmed by BET analysis. UV–Vis analysis was used to show a reduction in the band gap of Fe doped TiO_2/graphene sheets compared to commercial TiO_2. By increasing the amount of Fe, the band gap decreased to the visible region with 0.6% Fe/TiO_2 being optimum, similarly confirmed by PL spectra. Photocatalytic activity of synthesized catalysts was successfully examined by the photodegradation of model environmental endocrine disruptors (E2) under solar visible irradiation. This work suggests that high porous, visible-light photocatalysis has tremendous potential for the development of an environmentally sustainable treatment process using sunlight in place of an artificial light source, since visible light comprises a much larger portion of the solar spectrum than UV light.

Acknowledgments

This work was financially supported by the Canadian Natural Science and Engineering Research Council (NSERC) and the Canadian Foundation for Innovation (CFI).

Appendix A. Supplementary data

Supplementary data associated with this article can be found, in the online version, at doi:10.1016/j.apcatb.2011.08.012.

References

[1] R.R. Chowdhury, P. Charpentier, M.B. Ray, Industrial & Engineering Chemistry Research 49 (2010) 6923–6930.
[2] R.R. Chowdhury, P.A. Charpentier, M.B. Ray, Journal of Photochemistry and Photobiology A: Chemistry 219 (2011) 67–75.
[3] Y. Zhang, J. Zhou, B. Ning, Water Research 41 (2007) 19–26.
[4] X. Wang, J.C. Yu, C. Ho, Y. Hou, X. Fu, Langmuir 21 (2005) 2552–2559.
[5] I.K. Konstantinou, T.A. Albanis, Applied Catalysis B: Environmental 49 (2004) 1–14.
[6] J.R. Jennings, A. Ghicov, L.M. Peter, P. Schmuki, A.B. Walker, Journal of the American Chemical Society 130 (2008) 13364–13372.
[7] K.T. Meilert, D. Laub, J. Kiwi, Journal of Molecular Catalysis A: Chemical 237 (2005) 101–108.
[8] J. Tang, J.R. Durrant, D.R. Klug, Journal of the American Chemical Society 130 (2008) 13885–13891.
[9] G. Fu, P.S. Vary, C.-T. Lin, The Journal of Physical Chemistry B 109 (2005) 8889–8898.
[10] Y.D. Wang, G.J. Liu, et al., Advanced Functional Materials 18 (2008).
[11] Y. Furubayashi, T. Hitosugi, Y. Yamamoto, K. Inaba, G. Kinoda, Y. Hirose, T. Shimada, T. Hasegawa, Applied Physics Letters 86 (2005) 252101–252103.
[12] J. Wang, R. Limas-Ballesteros, T. Lopez, A. Moreno, R. Gomez, O. Novaro, X. Bokhimi, The Journal of Physical Chemistry B 105 (2001) 9692–9698.
[13] Z. Ambrus, N. Balazs, T. Alapi, G. Wittmann, P. Sipos, A. Dombi, K. Mogyorósi, Applied Catalysis B: Environmental 81 (2008) 27–37.
[14] K. Nagaveni, M. Hegde, G. Madras, The Journal of Physical Chemistry B 108 (2004) 20204–20212.
[15] S. Fukahori, H. Ichiura, T. Kitaoka, H. Tanaka, Environmental Science & Technology 37 (2003) 1048–1051.
[16] A.M. Turek, I.E. Wachs, E. DeCanio, The Journal of Physical Chemistry 96 (1992) 5000–5007.
[17] J. Aguado, R. van Grieken, M.J. Lopez-Munoz, J. Marugán, Applied Catalysis A: General 312 (2006) 202–212.
[18] J. Matos, A. García, P.S. Poon, Journal of Materials Science (2010) 1–11.
[19] J. Matos, A. Garcia, T. Cordero, J.M. Chovelon, C. Ferronato, Catalysis Letters 130 (2009) 568–574.
[20] K. Woan, G. Pyrgiotakis, W. Sigmund, Advanced Materials 21 (2009) 2233–2239.
[21] D. Wang, D. Choi, J. Li, Z. Yang, Z. Nie, R. Kou, D. Hu, C. Wang, L.V. Saraf, J. Zhang, ACS Nano 3 (2009) 907–914.
[22] H. Zhang, X. Lv, Y. Li, Y. Wang, J. Li, ACS Nano 4 (2009) 380–386.
[23] Y.-B. Tang, C.-S. Lee, J. Xu, Z.-T. Liu, Z.-H. Chen, Z. He, Y.-L. Cao, G. Yuan, H. Song, L. Chen, L. Luo, H.-M. Cheng, W.-J. Zhang, I. Bello, S.-T. Lee, ACS Nano 4 (2010) 3482–3488.
[24] M.J. McAllister, J.L. Li, D.H. Adamson, H.C. Schniepp, A.A. Abdala, J. Liu, M. Herrera-Alonso, D.L. Milius, R. Car, R.K. Prud'homme, Chemistry of Materials 19 (2007) 4396–4404.
[25] H.C. Schniepp, J.L. Li, M.J. McAllister, H. Sai, M. Herrera-Alonso, D.H. Adamson, R.K. Prud'homme, R. Car, D.A. Saville, I.A. Aksay, The Journal of Physical Chemistry B 110 (2006) 8535–8539.
[26] I.V. Lightcap, T.H. Kosel, P.V. Kamat, Nano Letters 10 (2010) 577–583.
[27] P.V. Kamat, The Journal of Physical Chemistry Letters 1 (2009) 520–527.
[28] T.N. Lambert, C.A. Chavez, B. Hernandez-Sanchez, P. Lu, N.S. Bell, A. Ambrosini, T. Friedman, T.J. Boyle, D.R. Wheeler, D.L. Huber, The Journal of Physical Chemistry C 113 (2009) 19812–19823.
[29] R. Sui, A.S. Rizkalla, P.A. Charpentier, Crystal Growth & Design 8 (2008) 3024–3031.
[30] R.A. Lucky, P.A. Charpentier, Advanced Materials 20 (2008) 1755–1759.
[31] R.A. Lucky, P.A. Charpentier, Science of Advanced Materials 1 (2009) 167–174.
[32] R.A. Lucky, P.A. Charpentier, Applied Catalysis B: Environmental 96 (2010) 516–523.
[33] N.W. Pu, C.A. Wang, Y. Sung, Y.M. Liu, M.D. Ger, Materials Letters 63 (2009) 1987–1989.
[34] L. Staudenmaier, Berichte der Deutschen Pharmazeutischen Gesellschaft 31 (1898) 1481.
[35] R. Sui, A.S. Rizkalla, P.A. Charpentier, The Journal of Physical Chemistry B 110 (2006) 16212–16218.
[36] L. Miao, P. Jin, K. Kaneko, A. Terai, N. Nabatova-Gabain, S. Tanemura, Applied Surface Science 212 (2003) 255–263.
[37] C.N. Banwell, E.M. McCash, Fundamentals of Molecular Spectroscopy, McGraw-Hill, London, 1983.
[38] G.D. Gilliland, Materials Science and Engineering: R: Reports 18 (1997) 99–399.
[39] K. Fujihara, S. Izumi, T. Ohno, M. Matsumura, Journal of Photochemistry and Photobiology A: Chemistry 132 (2000) 99–104.
[40] R.D. Shannon, J.A. Pask, Journal of the American Ceramic Society 48 (1965) 391–398.
[41] J. Choi, H. Park, M.R. Hoffmann, The Journal of Physical Chemistry C 114 (2009) 783–792.
[42] K.N. Kudin, B. Ozbas, H.C. Schniepp, R.K. Prud'Homme, I.A. Aksay, R. Car, Nano Letters 8 (2008) 36–41.
[43] W. Zhang, Y. He, M. Zhang, Z. Yin, Q. Chen, Journal of Physics D: Applied Physics 33 (2000) 912.
[44] S. Kelly, F.H. Pollak, M. Tomkiewicz, The Journal of Physical Chemistry B 101 (1997) 2730–2734.
[45] J. Zhu, J. Ren, Y. Huo, Z. Bian, H. Li, The Journal of Physical Chemistry C 111 (2007) 18965–18969.
[46] O. Akhavan, Carbon 48 (2010) 509–519.
[47] J.C. Yu, Ho Yu, Jiang, Zhang, Chemistry of Materials 14 (2002) 3808–3816.
[48] Y. Yao, G. Li, S. Ciston, R.M. Lueptow, K.A. Gray, Environmental Science & Technology 42 (2008) 4952–4957.
[49] R. Czerw, B. Foley, D. Tekleab, A. Rubio, P.M. Ajayan, D.L. Carroll, Physical Review B 66 (2002) 033408.